Multi-method field detection of map-scale faults and their parameters: Case study from the Vikartovce fault (Western Carpathians)

FRANTIŠEK MARKO[1,✉], ANDREJ MOJZEŠ[2], VOJTECH GAJDOŠ[3], KAMIL ROZIMANT[2], MARIÁN DYDA[6], VLADIMÍR BEZÁK[4], SLAVOMÍR DANIEL[5], IVETA SMETANOVÁ[4], BIBIANA BRIXOVÁ[2], IVAN ZVARA[2] and ERIK ANDRÁSSY[2]

[1]Comenius University in Bratislava, Faculty of Natural Sciences, Department of Geology and Paleontology, Ilkovičova 6, 842 15 Bratislava, Slovakia; ✉frantisek.marko@uniba.sk
[2]Comenius University in Bratislava, Faculty of Natural Sciences, Department of Engineering Geology, Hydrogeology and Applied Geophysics, Ilkovičova 6, 842 15 Bratislava, Slovakia; andrej.mojzes@uniba.sk
[3]IGC IngGeoCom Ltd., Bajkalská 9, 831 04 Bratislava, Slovakia
[4]Earth Science Institute, Slovak Academy of Sciences, Dúbravská cesta 9, 845 28 Bratislava, Slovakia
[5]Koral Ltd., Nad medzou 2, 052 01 Spišská Nová Ves, Slovakia
[6]Comenius University in Bratislava, Faculty of Natural Sciences, Department of Mineralogy, Petrology and Economic Geology, Ilkovičova 6, 842 15 Bratislava, Slovakia

Abstract: This research tests multi-method field survey for detecting fault parameters in a known fault structure interpreted on geological maps. The research was focused on detecting the Vikartovce fault and its inclination which is crucial for its genetic and kinematic interpretation. The chosen Vikartovce fault is a genetically related dislocation to the Sub-Tatras fault which is a major boundary fault in the Vysoké Tatry Mts. asymmetric horst. The Vikartovce fault can serve as a proxy for the evolution and physical and structural parameters of the Sub-Tatras fault which is difficult to study in the field because of thick Quaternary glaci-fluvial deposition cover. We applied a multi-method approach based on geophysical field surveys to detect the Vikartovce fault´s parameters. We combined ten field geophysical survey methods with soil and indoor radon emanometry and mercurometry along five profiles crosscutting the fault trace. These methods confirmed the presence of a fault between the Kozie chrbty ridge and the Paleogene sediments of the Hornád depression, described as the Vikartovce fault, and provided precise data on its geometry. This fault interface is represented by two major tightly spaced parallel north dipping reverse faults, tilted to almost a vertical position with an approximately 8 to 30 m wide fault damage zone and at least 1.5 km confirmed depth range.

Keywords: fault focused research , geophysical survey, soil emanometry, Vikartovce fault, Western Carpathians

Introduction

Precise data on fault localization and its parameters are beneficial for geological science, societal urban planning and health-risk assesment. These faults are usually interpreted on geological maps from mapped discontinuities of geological units and geomorphological features. Fault traces are often masked by the Quaternary cover sediments and vegetation which complicates their interpretation in maps, which used to be approximate. More efficient approach is needed to detect the surface fault trace and also the fault´s continuation to depth based on geophysical survey techniques. Several geophysical methods with shallow depth range up to 40 m and the controlled source audio-frequency magnetotelluric method with up to 1 500 m depth hit were applied to fulfil the goals.

One from the most attractive topics of the Western Carpathians Neo-Alpine tectonic evolution is the origin of the Vysoké Tatry Mts. (VT, Fig. 1). These have a relatively small area with typical high mountain altitude over 2600 m a. s. l. The following two concepts compete in explaining the VT block uplift.

The most widely accepted is the transpressional concept (as in Sperner 1996; Sperner et al. 2002) where the Vysoké Tatry Mts. block was uplifted, pushed-up as a xenomorph horst along the south-vergent Sub-Tatras boundary reverse fault (STAF) which dipped to the north. This was caused by transpression operating in the wide sinistral strike-slip brittle shear zone which contains the VT (Marko et al. 2017). Marko (1996) and Jurewicz (2005) then proposed the alternative concept of VT origin from block tilting. This was rimmed from the south by the Sub-Tatras boundary fault which dipped to the south and operated as a normal fault (Gross 1973; Maheľ 1986). This scenario could be supported by following the Neo-Alpine geodynamic context. After eastward migration of the Carpathian active front, the collision at this part of

the Carpathians induced intense E–W compression (Decker et al. 1993; Peresson & Decker 1997; Vass 1998). This stress field also affected the Carpathians interior, and its far-field effect could have been sufficient to create the E–W normal faults which could control block tilting in the final stages of Neo-Alpine evolution.

Both concepts have strong and weak aspects. The transpressional concept is well supported structurally, but it does not consider the superficial Mesozoic cover and nappe units north-ward plunge. In contrast, the tilting concept explains the arrangement of the Mesozoic superficial units tilted with their basement, but it is questionable whether this tilting alone could create such a large uplift (Twiss & Moores 1992; Janák et al. 2001). However, the Sub-Tatras fault has a dominant role in both these contrasting concepts of VT origin. This fault (STAF) operated as a north-dipping south-vergent reverse fault or south-dipping normal fault.

Despite their importance, the geometry and kinematics of the Sub-Tatras fault still remain unresolved despite many modern structural and geophysical studies and crustal architecture modelling (Tomek 1993; Bielik et al. 2006; Udič 2010; Pašteka et al. 2017 and Bezák et al. 2018). In addition, it is almost impossible to study the Sub-Tatras fault in-situ due to a few hundred metres thick Quaternary fluvio-glacial deposits covering the entire surface map trace of this fault (Lukniš 1973; Nemčok et al. 1993, 1994).

Fortunately, we can observe a similar tectonic style at the Kozie chrbty ridge. This comprises an uplifted and/or tilted block of Permian-Mesozoic basement units rimmed to the south by the Vikartovce fault (VIF – Fig. 1). The VIF has the same course as the STAF and we presume that it has the same inclination and kinematics, being genetically linked to the latter. Therefore, we consider the VIF a STAF "sibling", which reflects STAF evolution and has the similar geometry. In addition, the VIF dimensions and geological context are readily available for field geophysical survey and relatively easy to map. This inspired us to choose the VIF as our pilot research target that can serve as a proxy for the Sub-Tatras fault.

Apart from the geological tasks' formulation and the use of a relatively wide assemblage of geophysical techniques to solve them we were also trying to formulate the most effective fault survey methodology based on our field experience. It is generally known that some of geophysical techniques are more, while others are less competent to give valuable information on fault´s detection and its parameters (Mareš et al. 1983) and we set as one target of our work to verify this issue in practice and use the verified procedure in future works.

And finally, to fulfil the last important target of our research project – study of the environmental impacts of Western Carpathian faults – we performed the indoor radon activity concentration monitoring in the Vydrník village to verify the expected presence of a nearby fault (Mojzeš et al. 2017; Smetanová et al. 2022) and to assess the inhabitants' exposure to radon gas released through it.

Geological setting

The Cretaceous Paleo-Alpine structure of the Inner Western Carpathians – IWC (sensu Biely 1989 and Bezák et al. 2004) is affected by the populations of younger NE, NW, N–S, and E–W map-scale faults.

Among the E–W faults the most prominent are the deep-seated crustal block bounding discontinuities of the Hurbanovo–Dijósjenő and Rožňava faults. Figure 1 depicts the more shallow, upper crustal E–W faults, including a subject of our interest, the Sub-Tatras and Vikartovce faults.

The Vikartovce fault (VIF) is situated at the southern foot of the Kozie Chrbty mountain ridge and delineates a tectonic contact with the Hornád depression. This ridge is rimmed by the Neogene Hornád and Poprad depressions from the south and north, respectively. They are both created by down-thrust remnants of Paleogene basin. The boundary between the ridge and Hornád depression Paleogene sediments is morphologically distinct and appears perfectly linear on the maps.

Besides the Neo-Alpine activity of the VIF, neotectonic Pliocene–Quaternary movements are also reported owing to its topographical linearity, the occurrence of fault scarps and travertine distribution along its eastern continuation in the Sivá brada (Maglay et al. 1999; Sůkalová 2010; Vojtko et al. 2011 and Pivko & Vojtko 2021). Marko et al. (2010) and Vojtko et al. (2011) postulate a Quaternary age of its last activity while other authors highlight its influence on drainage networks (Roth 1938; Mičian 1962; Lukniš 1973 and Jakál 1992).

While fault control of the Kozie chrbty ridge southern boundary is geomorphologically evident, it is also possible that the Hornád depression, filled with Paleogene sediments, results from the natural catchment of the Paleogene sea-bay created during the Late Cretaceous rather than from the VIF dip-slip activity (Keith et al. 1991). However, the fault concept strongly prevails in both the literature and geological maps (Marschalko et al. 1966; Gross et al. 1999; Mello et al. 2000; Bezák et al. 2004, 2008; Vojtko et al. 2011).

Figure 2A and B depicts the Kozie chrbty horst emerging between the Poprad and Hornád depressions along the VIF. This is created by the Permian–Lower Triassic volcano-sedimentary complex of the Malužiná Formation which is referred to as the Ipoltica Group of the Hronic nappe unit, underlying the sediments of the Inner Carpathian Paleogene basin (ICPB) in the Hornád and Poprad depressions (Vozárová & Vozár 1988).

The following creations are also noted: (1) the Malužiná group is created by massive bodies of melaphyre tholeitic basalts with a complex of predominantly siliciclastic sediments of variegated sandstones, arcoses, shales, and intercalations of carbonates, evaporites and lesser basalts, andesites and their tuffites, (2) the upper part of the Kravany member of siliciclastic sedimentary sequence in the vicinity of the Vikartovce fault then comprises known occurrences of post-sedimentary uranium mineralization, (3) the Inner Carpathian Paleogene sedimentary fill forms Subtatric Group of the Hornád depression (Gross et al. 1984). This is created
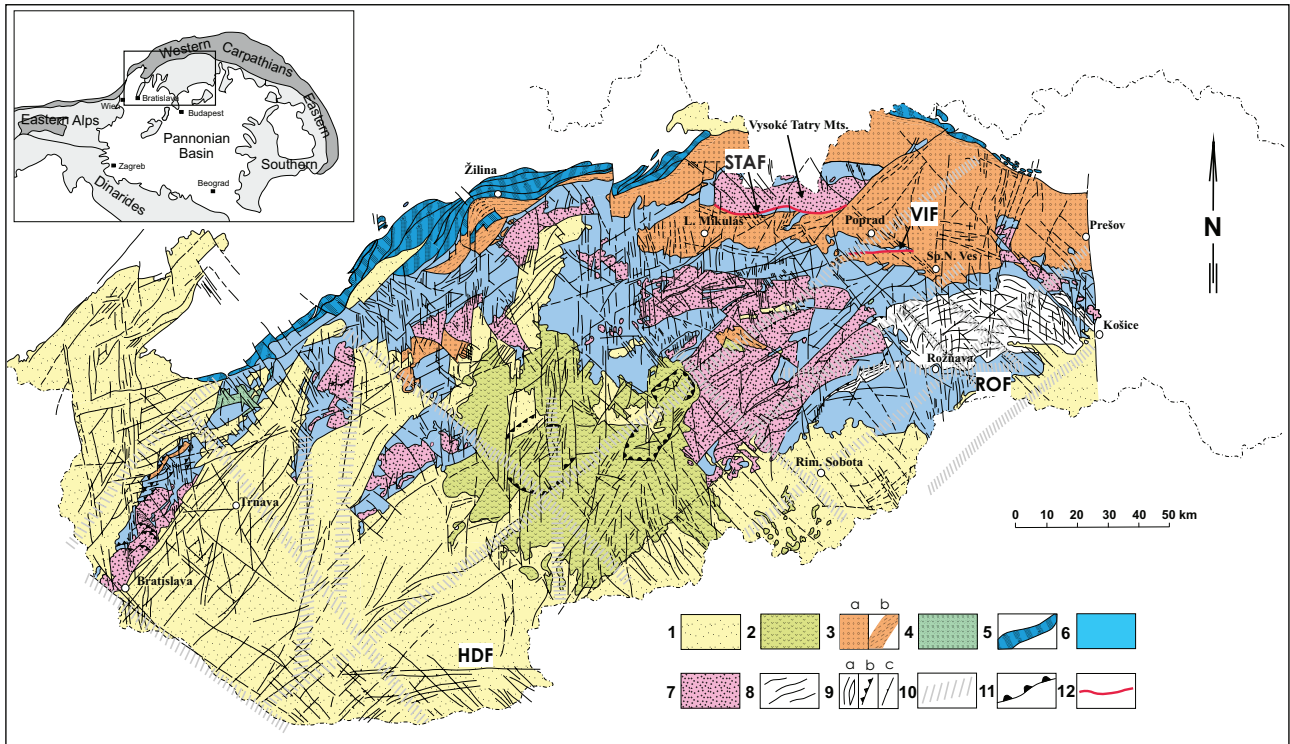
Fig. 1. Fault network of the Inner Western Carpathians (Marko 2002) . Explanations: 1 – Neogene sediments, 2 – products of Neogene volcanism, 3 – Inner Carpathian Paleogene Basin sediments (ICPB-Subtatric Group): a) unfolded, b) folded, 4 – Upper Cretaceous sediments (Gosau Group), 5 – Pieniny klippen belt unit, 6 – undivided Mesozoic nappe and cover units including Late Paleozoic complexes, 7 – undivided crystalline basement, 8 – Gemeric unit, 9 – faults: a) non-specified, b) reverse, c) normal, 10 – deep geophysically detected crustal discontinuities, 11 – extensional faults rimming volcanic calderas, 12 – investigated faults. Abbreviations: VIF – Vikartovce fault; STAF – Sub-Tatras fault; HDF – Hurbanovo–Dijósjenő fault; ROF – Rožňava fault.

Fig. 2. A — Kozie chrbty ridge panoramic view from the south. Vikartovce fault is situated on the pediment of the horst. **B —** View to the Kozie chrbty ridge from the south near Vydrník village. Behind are the Vysoké Tatry mountain peaks, which create another horst.

by the Middle-Upper Eocene transgressive basal clastics, coarse and fine-grained graywackes and siltstones, claystones, marlstones, carbonates and flysch siltstones and graywackes (Marschalko et al. 1966) and finally, (4) the Vikartovce fault connects with the Huty Formation of the Inner Carpathian Paleogene basin fill created by intercalated beds of claystones, siltstones and fine-grained sandstones.

There are also Quaternary – Late Pleistocene to Holocene deposits which mostly occur on the Hornád depression Paleogene formations. The most common of these deposits are fluvial and deluvial slope sediments. While fluvial deposits are mostly on high, medium and low terraces along the Hornád River, deluvial slope loams, stony screes and proluvial loamy gravels and sandy loams are deposited along the foot of the Kozie Chrbty ridge (Marschalko et al. 1966; Mello et al. 2000). These latter deposits often cover the estimated VIF map trace between Kravany, Spišský Štiavnik and Vydrník villages.

Research methods

Designated profile lines across the expected fault trace, indicated also by dowsing, were selected in specific areas for further geophysical measurements. Field geophysical surveys detected fault position and its properties. This was accomplished by the following methods: Dipole ElectroMagnetic Profiling (DEMP), Electrical Resistivity Tomography (ERT), Vertical Electrical Sounding (VES), Self-Potential (SP) technique, Very Low Frequency (VLF) electromagnetic method, Ground Magnetometry (GM), Controlled Source Audiofrequency MagnetoTellurics (CSAMT), Seismic Refraction Tomography (SRT), soil and indoor Radon Emanometry (Rn soil and Rn indoor), soil Mercurometry (Hg soil) and Gamma-Ray Spectrometry (GRS).

These methods resolved the VIF dip direction and damage zone cross-section characteristics. The following five profiles were chosen for detailed field research: Kravany, Spišské Bystré, Hranovnica–Dubina, Spišský Štiavnik and Vydrník (Fig. 3). All profiles were arranged perpendicular to the VIF strike identified by reconnaissance dowsing, and then compared with published geological maps. Finally, indoor radon activity concentration was monitored for one year in 22 selected dwellings in the Vydrnik village in order to determine radon gas emission from the VIF damage zone.

Dipole Electromagnetic Profiling Method (DEMP) records artificially induced electromagnetic fields in rock environments. The measuring apparatus is calibrated in the way that the measured values of the entire EM field resulting from the interaction between the primary instrument component and the secondary one induced in the rock environment are linearly dependent on the electrical conductivity of the rock environment. The apparatus is designed as a compact tube with measuring antennas installed, and transmission enables measurement of the required horizontal step-changes in the apparent resistivity of the approximately 6-metre-thick rock surface layer. Measurements performed in a flat measuring network enable the compilation of a resistance map from the measurement results and resistance inhomogeneities are manifested by a significant anomalous effect. The CMD-Explorer mapped the rock conductivity at 1.5, 3 and 7 m depths along the measured profiles and provided rapid spatial localization of the maximum resistivity inhomogeneities at those depths (CMD-Explorer – GF Instruments, Czech Republic).

Electrical Resistivity Tomography Method (ERT) is a basic method for compiling vertical resistivity sections and geophysical monitoring by combining resistance profiling and vertical electrical sounding. The measurement is performed by an electrode series stretched over dense steps of approximately 2–5 m. The computer-controlled current transmission and voltage reception provide a relatively detailed picture of apparent vertical section resistivity distributed along the measured profile. Subsequent computer processing by Res2DInv software enables measured data transformation into a set of actual resistivity values, and we thereby obtain an image of the actual rock environment structure. Repeated measurements then made it possible to detect even small changes in the investigated rock environment and assess the development of the influence of various factors on this environment. The comparative and supporting evidence by ERT vertical cross-section generation along the profiles selected by the DEMP process was provided by the **Vertical Electrical Sounding Method (VES)**. Here, the ARES instrument was used for ERT and VES measurements. (ARES instrument from GF Instruments, Czech Republic)

Self-potential Method (SP) is an electrochemical method which exploits spontaneous polarization of natural conductors. This is based on the study of local natural electric fields, and these especially include those with electro-chemical, filtration and diffusive origin. Filtration fields are most important in fault-issue solutions because they are generated by groundwater filtration from the rocks. This especially occurs in mountainous relief conditions and river valleys. The elevated areas from which the waters filter to lower regions have negative potential compared to the valley areas (Mareš et al. 1984). Two non-polarizing electrodes, wiring and the ARES instrument provided Self-Potential measurements.

Very Low Frequency Method (VLF) is an electromagnetic procedure using artificial electromagnetic fields from powerful navigation transmitters in the 10 to 150 kHz VLF band (Mareš et al. 1984). The measured parameters are usually ratios of actual and imaginary components of the vertical to horizontal magnetic fields resulting from primary and secondary magnetic field interaction (Geofyzika, n.p. 1978). The homogeneity of the primary electromagnetic field is often disrupted by local geological conductors, and this method is mostly used for location and resistivity mapping of conductive geological structures such as those originating from tectonic disturbance and ore veins which then form rock boundaries. The measurements were performed in the 10–25 kHz band EDA 78 produced by Geofyzika, n.p. at Brno in Czechoslovakia. In addition, the available IXZ and ICV radio navigation stations still provide acceptable signals, despite many decommissioned transmitters (Milsom & Eriksen 2011).

Ground Magnetometry Method (GM) is a rapid and cost-effective geophysical method for studying variations in the Earth's natural magnetic field. This procedure exploits the magnetic contrasts in sub-surface rocks. Many rocks and minerals are weakly magnetic or are magnetized by induction, and these cause spatial perturbations or anomalies in the Earth's magnetic field. The GM methods are based on measuring the magnetic effects produced by varying concentrations of ferromagnetic minerals, in geological formations. These include magnetite, and the sedimentary rocks generally have very small susceptibility compared to igneous or metamorphic rocks. Most magnetic surveys are therefore designed to map structures on and within the basement, or for direct detection of magnetic minerals. The GM procedure measures the Earth's total magnetic field intensity in nano-Teslas (nT), and the PM2 single sensor proton precession magnetometer was used for these measurements (Geofyzika Brno, Czechoslovakia).
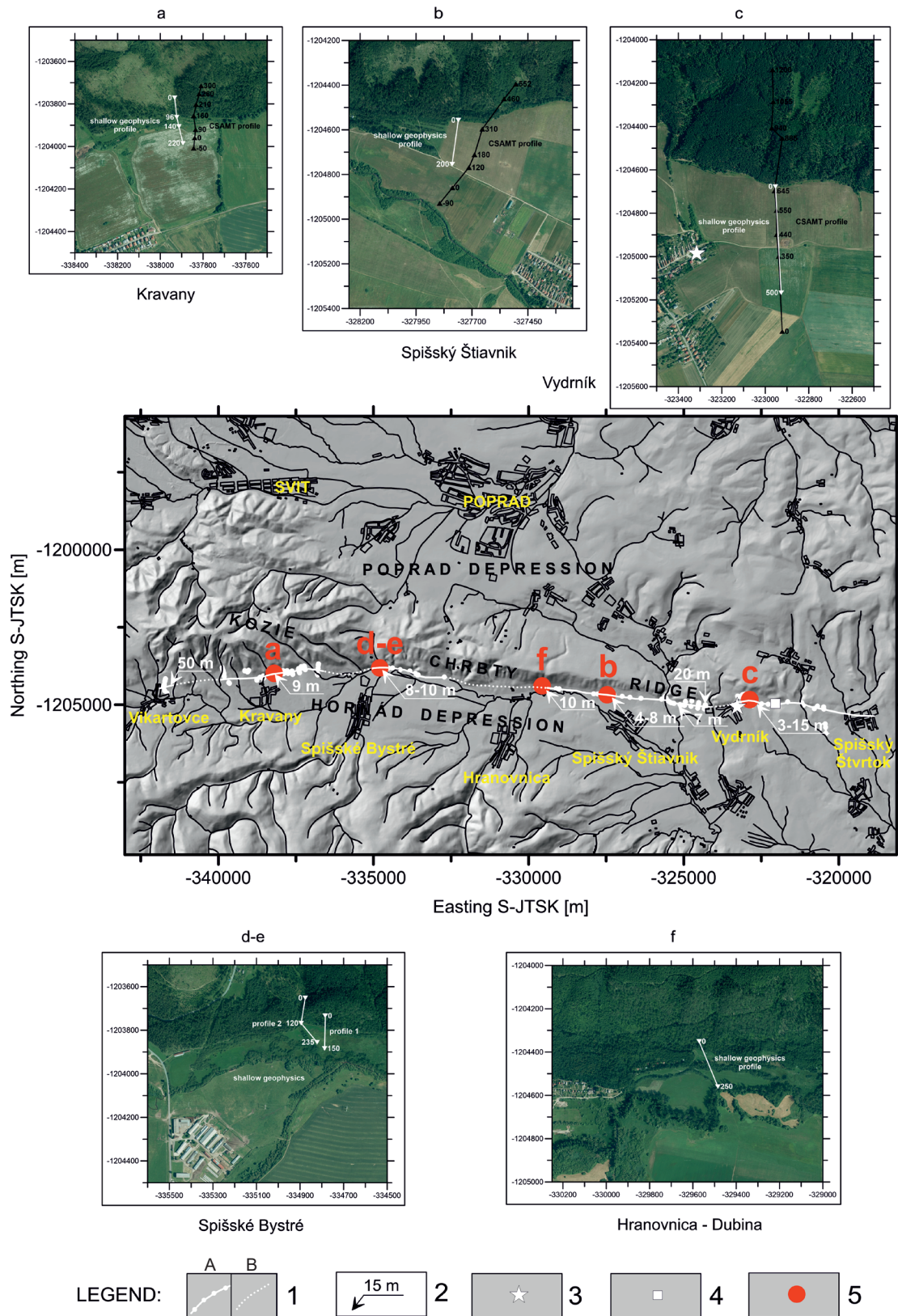
Fig. 3. Localization of CSAMT and shallow geophysics profiles and VIF mapping results from dowsing. 1 – a) VIF trace detected and mapped by dowsing, b) estimated VIF trace; 2 – Width of the fault damage zone detected by dowsing; 3 – The highest indoor radon concentration in the Vydrník village; 4 – Occurrence of travertine; 5 – Survey profiles localization: a – Kravany, b – Spišský Štiavnik, c – Vydrník, d and e – Spišské Bystré, f – Hranovnica–Dubina (topographic background: GCI&NFC, 2017-2019).

The profile positions were set at 5 m sampling intervals, as in ERT measurements.

Audio-Magneto-Telluric Profiling Method (AMT) provides detailed characteristics of selected fault structures. The **Controlled Source Audio-frequency MagnetoTellurics (CSAMT)** is a frequency-domain electromagnetic sounding technique which employs a fixed grounded dipole as an artificial signal source. This source provides a stable, dependable signal and it gives higher-precision and more economical measurements than those usually obtained from natural-source measurements in the same spectral bands.

The combined multi-purpose Metronix TXM-22 geophysical transmitter and TXB-07 controller provide the control source. The output current is fed into 3-electrode triangular nests which enabled current vector rotation in all directions. A total of 5–8 deeply grounded electrodes were set up, and salt-water addition decreased the transitional resistivity between the electrode and rock cover.

Here, base frequency defines the output signal frequency in the 1–8148 Hz range, and we employed far-field geometry where the magnetic and electric fields behave as plane waves. A standard receiver configuration lacking the Hz-component was applied with −25, +25 m NS and EW sensor spacing. The Ex, Ey, Hx, Hy phases and magnitudes were then measured and the ohmic sub-surface impedance was determined from the perpendicular components of the horizontal electric and magnetic fields.

The precise Global Positioning System (GPS) was used for time synchronization between the transmitter and receiver, and ZOND 2MT 2D inversion modelling software processed the data. Finally, the field AMT measurements and data processing were provided by Koral Ltd., Slovakia and the Geophysical Division of the Earth Science Institute of the Slovak Academy of Sciences.

Seismic Refraction Tomography Method (SRT) controls source seismic waves to determine the depth of seismic interfaces beneath the surface and the propagation velocity of seismic waves between interfaces (Lillie 1999). Seismic waves propagate from the source and the arrival of each wave is detected along the straight geophone line. The seismic shot-source is located at the beginning and end of a geophone line or, alternatively, it can be positioned along the geophone-spread or at a discrete distance from the end of the spread. The chosen shot-position provides adequate lateral resolution (Reynolds 1997). The seismic measurements were performed by 24-channel DMT equipment with 10 Hz vertical geophones and a hammer as the source. The measured data was processed in the Sandmeier (2017) Reflex Version 8.0 by refraction seismic processing. Finally, the created sub-surface environment velocity model was the initial model used for seismic refraction tomography, and this provided a continuous velocity gradient across the sub-surface.

Soil Radon Emanometry Method (Rn soil) is an atmo-geochemical technique based on measuring alpha radiation originating in soil air samples taken from the depth of approximately 0.8 m. Their immediate in situ analysis is by scintillation radon detector. This method provides the curve of ^{222}Rn activity concentration values in the near-surface horizon along the studied profile in kiloBecquerels per cubic metre (kBq·m^{-3}). These measurements help specify the fault position and the part most permeable to gases. The LUK 3R portable radon detector from SMM Prague in the Czech Republic was used for field measurements.

Indoor Radon Activity Concentration Monitoring (Rn indoor) is the integration measurement of ^{222}Rn activity concentration (Bq·m^{-3}) in houses near the VIF trace that was performed by a Ramarn track detector (State Institute of Radiation Protection, Prague, Czech Republic). The detectors were ideally placed in two inhabited rooms situated on the ground floor of a monitored house. Rooms in direct contact with the subsoil were preferred for monitoring, and detectors were changed after three months exposure. This procedure compared radon activity concentration changes throughout the year. A questionnaire and a flyer about this radon exposure were distributed to the inhabitants of the monitored houses.

Soil Mercurometry Method (Hg soil) is a further fundamental atmo-geochemical technique which determines parts/billion mercury content (ppb) in soil, air and water samples. Underground air samples from a 50–80 cm excavation hole were analysed in situ. The portable multi-functional atomic absorption spectrometer was employed for field measurements (RA-915M Mercury Analyser, producer: Lumex Instruments Canada). This was combined with Zeeman background correction and elimination of interference impurities, and the field mercurometry measurements and data processing were provided by Koral Ltd., Slovakia.

Gamma-Ray Spectrometry Method (GRS) provides valuable information on 4 measurements of gamma radiation from rock and soil. This is achieved with a portable 256-channel spectrometer with 0.347-litre volume NaI(Tl) scintillation detector and 12-channel embedded GPS receiver (Pico Envirotec Inc. 2014). These measurements were: the total gamma-ray activity in the form of the gamma dose rate equivalent in the air at 1 m elevation above the ground (in nanoSieverts per hour [nSv·h^{-1}]) and the ^{40}K, ^{238}U and ^{232}Th concentrations in the near-surface horizon. These latter measurements were recorded in percentage K and ppm eU and eTh. A bluetooth-connected handheld system controller and data logger enabled walking-mode survey with 1 Hz measurement frequency and approximately 2 m sampling distance. The profile measurement provides the curves along the studied profile crossing the fault line, and the method is sensitive to local litho-geochemical composition which specifies the geological zone. Measurements were performed by the Pico Envirotec PGIS-2 system.

Dowsing Fault Mapping Method (DFM). Although the physical principles of dowsing are still not known (Fiddick 2011; Kowalski 1996), pragmatic field scientists apply it as a complementary procedure for rapid indication of underground objects (e.g. Betz 1995; Landa & Kovalevsky 1997; Lohmann 1998; Daynes 2012; Moldovan et al. 2013). The human-detection dowsing procedure for fault mapping

was implemented by a collective of authors in 2015. This method provides rapid field detection and mapping trace and width of dislocations at the surface (Marko et al. 2015). It was performed as a simple field method supporting localization of geophysical measurements.

Field survey results

The combination of shallow depth research methods and deep range geophysical measurements detected Vikartovce map-scale fault parameters. Three field campaigns of shallow depth geophysical measurements along approximately 1600 metres in the five – Kravany, Spišské Bystré, Hranovnica–Dubina, Spišský Štiavnik and Vydrník profiles (Fig. 3) were carried out. Indoor Rn activity concentration (Rn indoor) on the VIF trace was monitored in 22 inhabited houses in the Vydrník village for one year. This confirmed elevated indoor radon activity concentration above the reference level of 300 Bq·m^{-3} in one house, and this approaches the high 370 ±55 Bq·m^{-3} value (Smetanová et al. 2019). The radon concentration is attributed to the VIF source, and this is supported by the existence of a mineral water spa operating in the house courtyard at the beginning of the 20th century. The final indoor radon measurement evaluation is the subject of a separate contribution (Smetanová et al. 2022).

The CSAMT measurements were determined along approximately 2200 metres of the Kravany, Spišský Štiavnik and Vydrník profiles (Fig. 3). The dowsing method supported all field survey procedures in fault detection.

CSAMT

CSAMT measurement results along the three survey profiles cross-cutting the VIF are displayed in cross-sections reaching 0.6 to 1.2 km depth, and they show the rock electrical resistivity (Fig. 4). The high resistivity contrast between the Kozie chrbty ridge horst and the ICPB Paleogene filling juxtaposed by the VIF enabled interpretation of the VIF interface in all three cross-sections. This was sub-vertical or 80° declined to the north in all cross-sections. The CSAMT cross-sections were also interpreted geologically and faults kinematically, accepting the up-to date knowledge concerning the geological architecture of the area established on the geological map (Mello et al. 2000).

Figure 4A and 4B show that the Kravany and Spišský Štiavnik cross-sections have the same tectonic style. There is also steep VIF north-dipping at the pediment of the southern slope of the Kozie chrbty ridge (with its surface placed at about 140 m in the Kravany profile and about 235–240 m in the Spišský Štiavnik profile). The ICPB bedrock of the Kozie chrbty ridge was along the VIF up-thrust, and the fault therefore has reverse kinematics. In addition, the parallel vertical fault with its surface trace located approximately 25 m away in the Kravany profile and about 60–65 m in the Spišský Štiavnik profile was detected tens-of metres south of the VIF in both

cross-sections. Further down-throw of ICPB filling in respect to its bedrock, reaching a magnitude of cca 200 m in Spišský Štiavnik and more than 400 m in Kravany, has happened along this fault.

Figure 4C shows that the Vydrník cross-section is more complex, with distinctive slumped blocks of high electrically resistive rocks of the Ipoltica group. They slipped south to the ICPB from the edge and top of the up-thrust horst. The structurally highest block could reflect a recent sliding cap of the Ipoltica horst up-thrust along the VIF. The slid block in deeper position created an anticline in the overlying Paleogene sedimentary sequence forming a trap for water and volatiles based on anomalous low resistivity of this structure.

The VIF is interpreted here as a vertical interface between the highly resistive Ipoltica group and lower resistive ICPB at approximately 900–950 m below the surface (Fig. 4C). The CSAMT traces this discontinuity to 2 km depth, and it accommodates uplift of the highly resistive northern block against the lower-resistive southern block. Another parallel sub-vertical fault is interpreted in CSAMT cross-section approximately 400 m south of the VIF. This highlights the rim of the thicker part of the Inner Carpathian Paleogene Basin. A similar structure is observed in the Kravany and Spišský Štiavnik profiles.

Shallow depth range geophysics

Geophysical and emanometry survey techniques were applied to five localities along short 100–400 m lines perpendicular to the VIF trace mapped by dowsing with the survey depth assumed up to the first tens-of-metres. Ground magnetometry, gamma-ray spectrometry and DEMP were initially performed to give an overview of the survey line. A part, or a few parts of such line, were then selected for detailed geophysical investigation by other geophysical methods with shallow depth range including both Rn and Hg soil emanometry methods that, as supposed, could also have deeper response. This was mainly based on lower DEMP resistivity values.

Dowsing

The tested procedure supported the above mentioned geophysical and emanometric surveys. The Vikartovce fault trace is often only estimated, and it is imprecisely drawn on geological maps. This is caused by Quaternary cover masking the surface fault trace. Our fault mapping provided rapid and precise field detection of VIF and its width. We have mapped the VIF intersection with the surface trace for 10.5 km in the surface topography between Kravany, Vydrník and Spišský Štvrtok villages, and the surface width of the VIF damage zone was established in the 6 to 30 m range (Fig. 3). Figure 5 highlights that this dowsing related VIF trace corresponds well with its actual position determined by CSAMT.
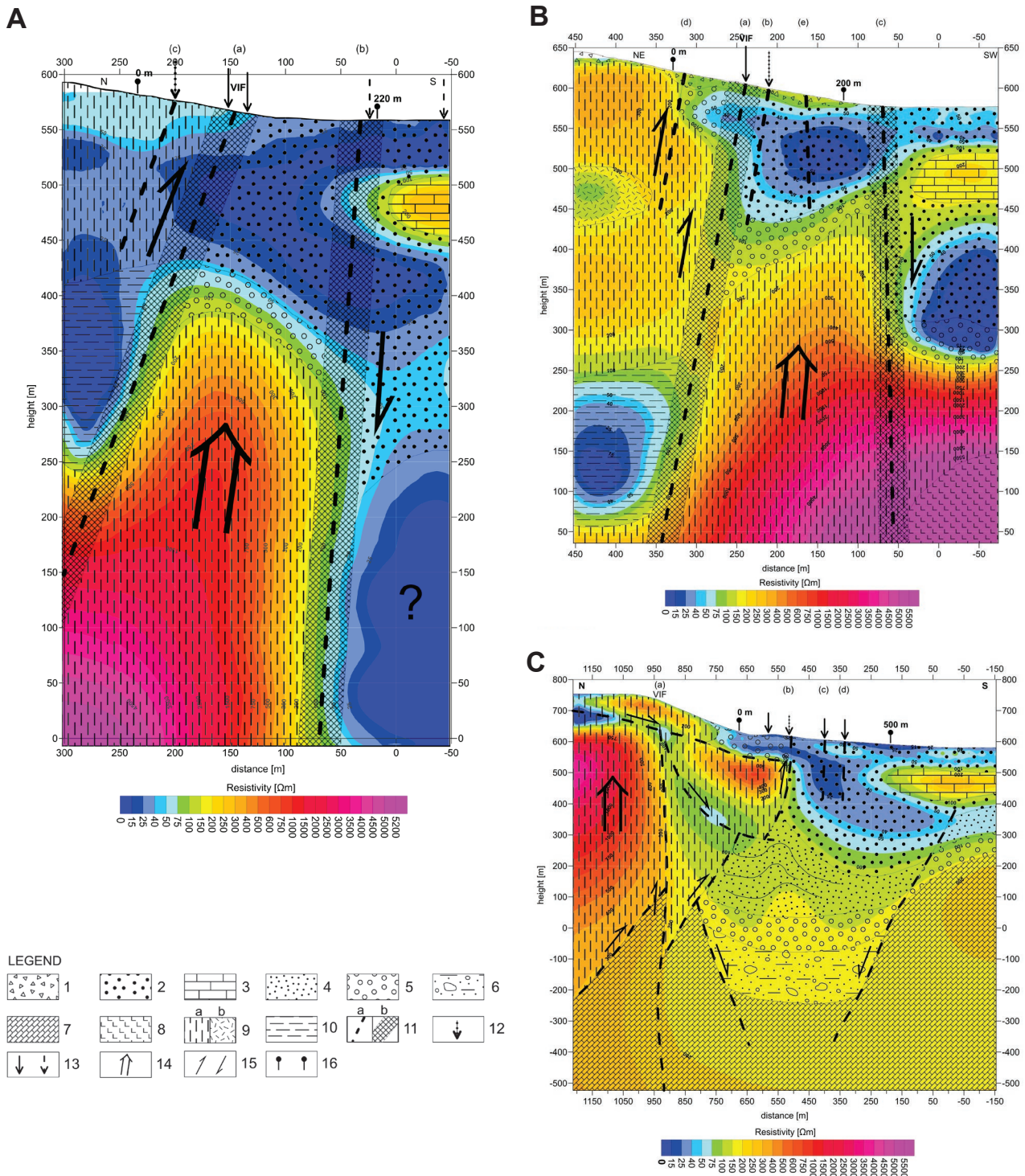
Fig. 4. Geologically interpreted CSAMT cross-sections: **A** — Kravany, **B** — Spišský Štiavnik, **C** — Vydrník. Explanations according to Mello et al. (2000) division: *Weathering cover sediments (Quaternary)* – 1. sandy-stony screes; *Subtatric Group (Paleogene)* – 2. claystones, silt-stones, sandstones (Huty Formation), 3. lumachelle limestone olistoliths (Huty Formation), 4. fine-grained sandstones and siltstones and con-glomerate layers (Tomášovce Member), 5. fine-grained conglomerates and sandstones (Borové Formation); *Gosau Group (Late Cretaceous)* – 6. polymict boulder conglomerates; *Ipoltica Group of Choč nappe (Permian)* – 7. sandstones, clayey shales (III-rd megacycle), 8. tholeite basalts and andesites, 9. a) sandstones, clayey shales, b) evaporites and carbonates (II-nd and III-rd megacycle), 10. low resistivity rocks satu-rated with water or disintegrated carbonates, evaporites; *Structural features* – 11. a) faults interpreted from CSAMT data, b) fault damage zones, 12. Vikartovce fault position interpreted in actual geological map at 1:50,000 (Mello et al. 2000), 13. fault position detected by dowsing mapping, 14. block dynamics, 15. fault kinematics, 16. surface geophysical profile marginal points. Geophysically detected single faults are distinguished by alphabet indications (a – VIFs.s., b, c, …) commented in the text.

Correlation of field survey results

Our field research detected the VIF and its parameters. The geophysical and emanometric measurements along the Kravany, Spišský Štiavnik and Vydrník profiles were calibrated in the unit scale, correctly positioned and juxtaposed in synthetic figures (Fig. 5). This enabled comparison of fault detection method results and evaluation of their accuracy and effectiveness. Geologically interpreted CSAMT cross-sections provided background for the shallow depth results comparison, and this procedure alone provided reliable and accurate detection of the VIF position in cross-sections. Finally, the shallow-depth methods were compared and evaluated whether or not they confirm the VIF position interpreted in the CSAMT cross-sections.

Figure 5A, B and C show results for Kravany, Spišský Štvrtok and Vydrník localities where CSAMT was measured as well, while Figure 5D, E and F show results of shallow depth range geophysics measurements for the Spišské Bystré and Hranovnica–Dubina localities where CSAMT was not measured. Geographical coordinates of survey profiles are given in Table 1.

Kravany profile (Fig. 5A)

The Kravany profile is the most western profile perpendicular to the Vikartovce fault strike, and here dowsing was combined with eight geophysical fault-detection methods along the profile line. All methods correlated, and they recorded two dislocations confirmed in the CSAMT cross section. These were the main subvertical VIF (a) and southern steeply north-dipping (b) faults (Fig. 4A).

The north-dipping VIF (a) depicted at approximately 140 m in this figure was accurately detected between 90 and 120 m by the highest soil radon anomaly (up to 50 kBq·m^{-3}) at 100–110 m, moderate positive VLF gradient anomaly at 105–130 m, lower DEMP and ERT resistivity values at 95–115 m, and also by visible offset at 100 m in the SRT cross-section (Fig. 5A). A sharp magnetic minimum at 100 m could be assigned to artificial material of the field road crossing the line at this place. The ERT cross-section in Figure 5A shows that this fault (a) forms the tectonic boundary between higher resistivity Permian sandstones in the northern part of the profile and lower resistivity Paleogene claystones in the southern portion. The subvertical interface dividing blocks of contrasting resistivities could be regarded as the structure (e.g. minor antithetic fault) related to the master (VIF s.s., a).

The southern sub-vertical fault (b) at approximately 25 m in Figure 4A is also clearly detected by the visible SRT cross-section offset at 180–200 m, weak soil Rn anomaly up to 20 kBq·m^{-3} at 190 m and by minimal positive VLF gradient Re(Hz) (Fig. 5A).

The VIF northern parallel offshoot (c) exists at 190–210 m in Figure 4A that fits very well with fault position in geological map (Mello et al. 2000). This is recorded in the station range between 20–40 m by the highest positive VLF gradient Re(Hz)

anomaly at 20–40 m, lower DEMP and ERT resistivity values at 25–40 m, slightly elevated soil Rn values (up to 14 kBq·m^{-3}) at 30–40 m and by an unimpressive magnetic disturbance (Fig. 5A). However, lower seismic velocities are indicated rather at around the 10 m level in the SRT cross-section.

The three faults, including the VIF, are synchronized in the CSAMT cross-section surface faults detected by both dowsing and geologically-mapped faults (Fig. 4A).

While the strong Figure 5A anomaly of gamma dose rate equivalent approaching 186 nSv·h^{-1} at the 40–50 m station can be construed as a northern VIF offshoot (c) between 20 and 40 m recording a tension fracture or a vein-sealed fault with uranium mineralization, it is more difficult to interpret the soil Hg curve.

Spišský Štiavnik profile (Fig. 5B)

The CSAMT cross-section at the Spišský Štiavnik profile (Fig. 4B) offers similar picture as that at the Kravany profile (Fig. 4A). The master VIF s.s. fault stationed at approximately 235–240 m (Fig. 4B) coincides perfectly with the dowsing results which rendered an 8–15 m wide East–West active strike zone, the relationship to the geological map is inconsistent. Here, Mello et al. (2000) VIF interpretation in the current geological map is almost 30 m south of that determined by both dowsing and CSAMT (Fig. 4B). Furthermore, the correlation between CSAMT related faults and shallow-depth geophysical and emanometric data is also imperfect.

The master VIF (a) is determined in Figure 5B at 70–85 m by low resistivity in the deeper part of the ERT cross-section, invariable DEMP resistivity values, a small positive VLF gradient Re(Hz) anomaly at about 80–85 m and a slightly vertical channel with lower SRT cross-section velocity. The fault detemined in the ERT cross-section forms the tectonic boundary between the northern Permian sandstones with higher resistivity and the southern Paleogene claystones with lower resisitivity (Fig. 5B). However, the cause of these resistivity differences is less clear than in the Kravany profile (Fig. 5A), and this is considered due to heterogeneous conditions during Quaternary deposition and the presence of thick Quaternary cover.

In contrast, the VIF drawn on the geological map (b) at approximately 210 m (Fig. 4B) is established by soil Rn emanometry as a wider zone of slightly elevated soil radon activity concentration between 105 and 120 m with values up to 20 kBq·m^{-3} (Fig. 5B). This is combined with decreased DEMP resistivity values in the same range and most likely with the middle soil mercurometry anomaly (Fig. 5B).

The steeply dipping VIF parallel southern reverse fault (c) interpreted in the CSAMT cross-section at approximately 60–65 m is outside surface geophysical measurement range (Fig. 4B).

The two VIF sub-parallel offshoots were detected by distinctive soil radon anomalies up to 94 kBq·m^{-3} at 20–40 m (d) and up to 63 kBq·m^{-3} at 160–170 m (e). These are accompanied by positive VLF gradient anomalies and lower DEMP
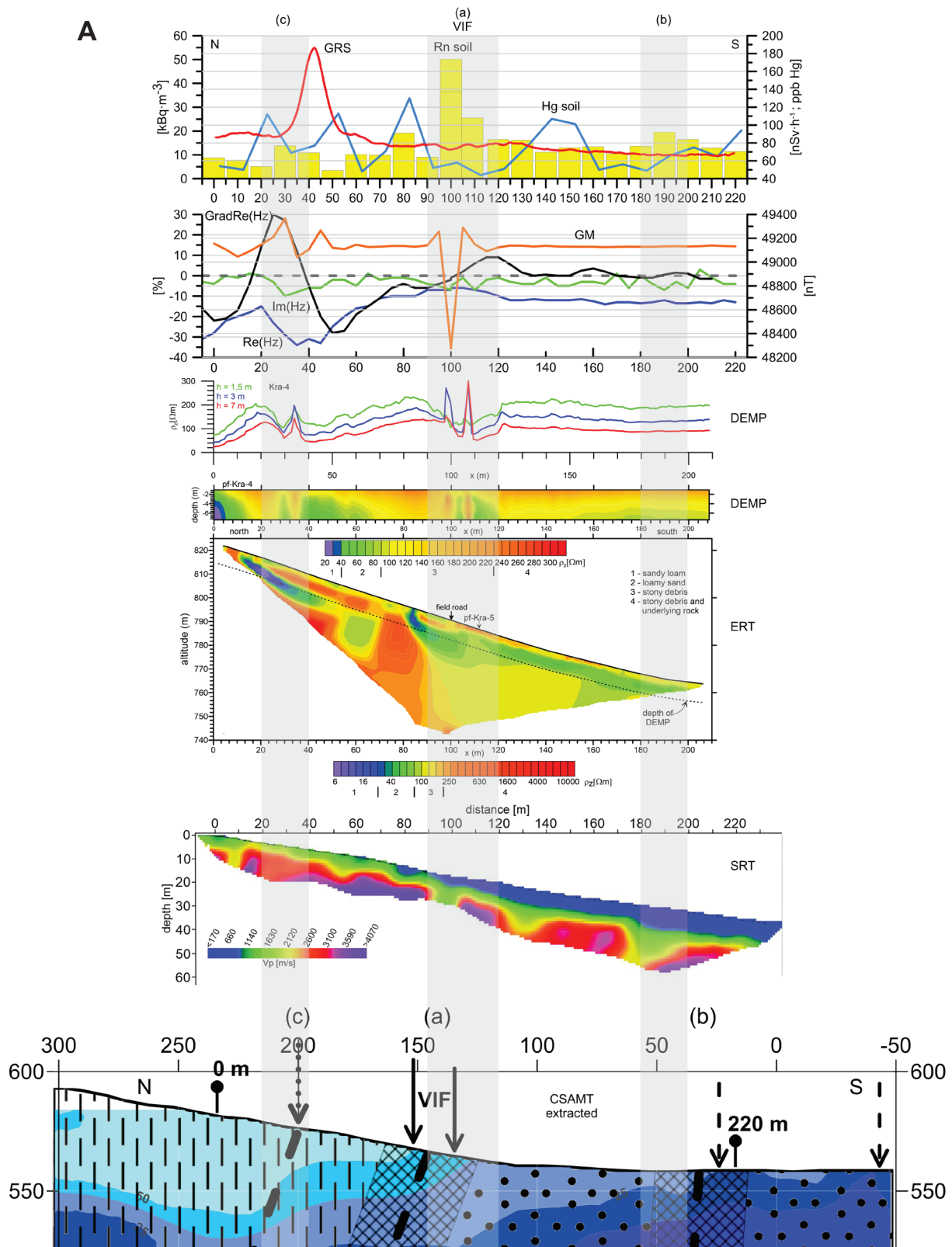
Fig. 5. Comparison of CSAMT related fault structures and shallow depth geophysical, emanometric and dowsing data. **A** — Kravany profile; **B** — Spišský Štiavnik profile; **C** — Vydrník profile; **D, E** — Spišské Bystré profiles; **F** — Hranovnica–Dubina profile. Geophysically detected single faults are distinguished by alphabet indications (a – VIFs.s., b, c, …) commented in the text. Grey transparent belts mark and connect multi-method indications of the same fault-discontinuity.
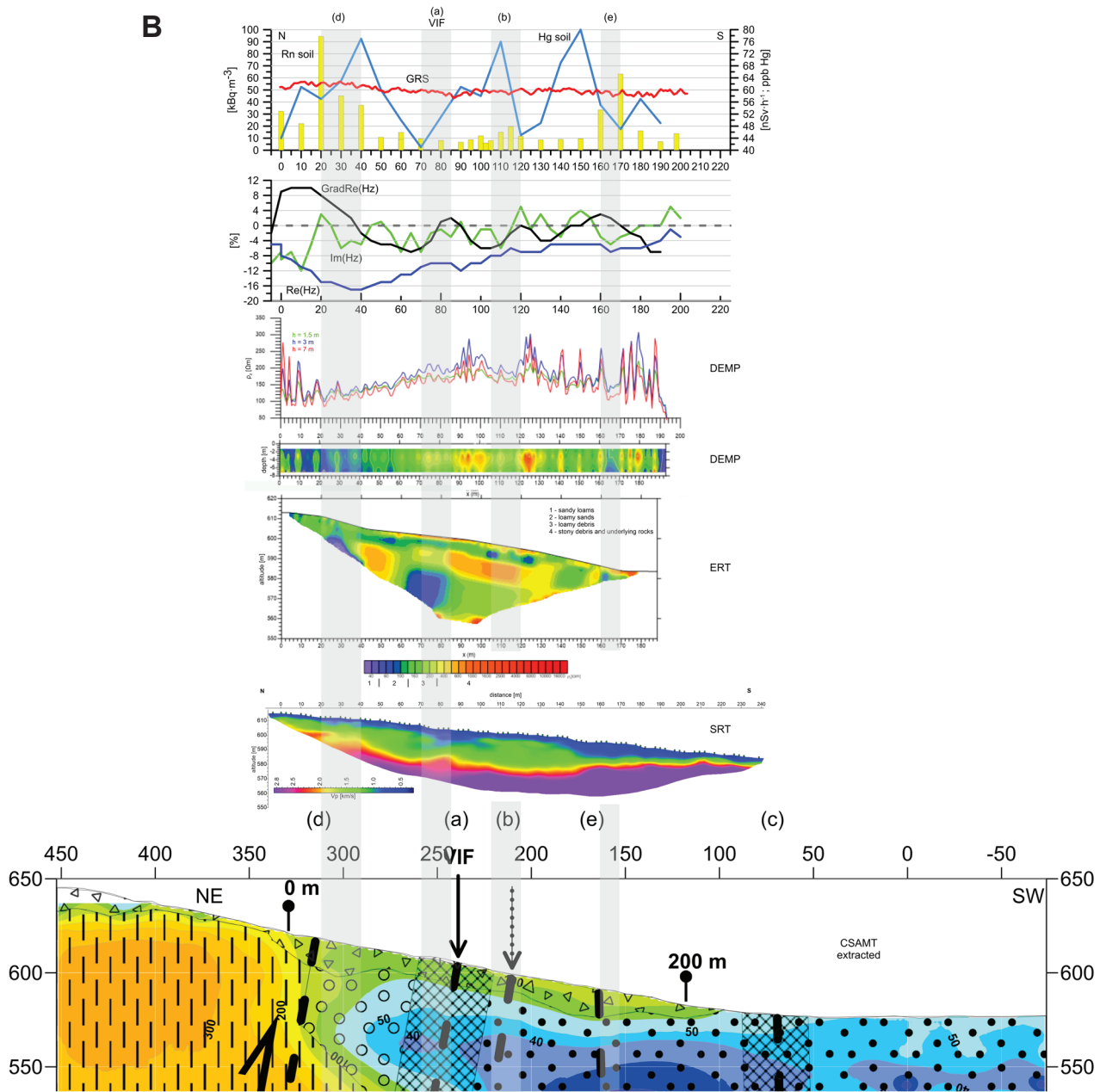
Fig. 5. (continued) Comparison of CSAMT related fault structures and shallow depth geophysical, emanometric and dowsing data. **A** — Kravany profile; **B** — Spišský Štiavnik profile; **C** — Vydrník profile; **D, E** — Spišské Bystré profiles; **F** — Hranovnica–Dubina profile. Geophysically detected single faults are distinguished by alphabet indications (a – VIFs.s., b, c, …) commented in the text. Grey transparent belts mark and connect multi-method indications of the same fault-discontinuity.

and ERT resistivity values. Finally, the 20–40 m stationing also has a high Hg soil anomaly and slightly lower SRT cross-section velocities of the bedrock (Fig. 5B).

Although the shallow-depth refraction seismic profile (SRT) does not precisely record the VIF zone, it distinguishes Quaternary cover depositions from the bedrock. Figure 5B depicts their maximum thickness at almost 20 m, and this large thickness explains controversial VIF recordings from many shallow depth geophysical methods. It also highlights

the homogeneous near-surface lithological material in the monotonous course of the gamma dose rate equivalent curve along the Spišský Štiavnik profile (Fig. 5B).

Vydrník profile (Fig. 5C)

All shallow depth measurements were made across the VIF trace interpreted in the geological map. These were followed by CSAMT measurement. Due to this fact and extreme terrain
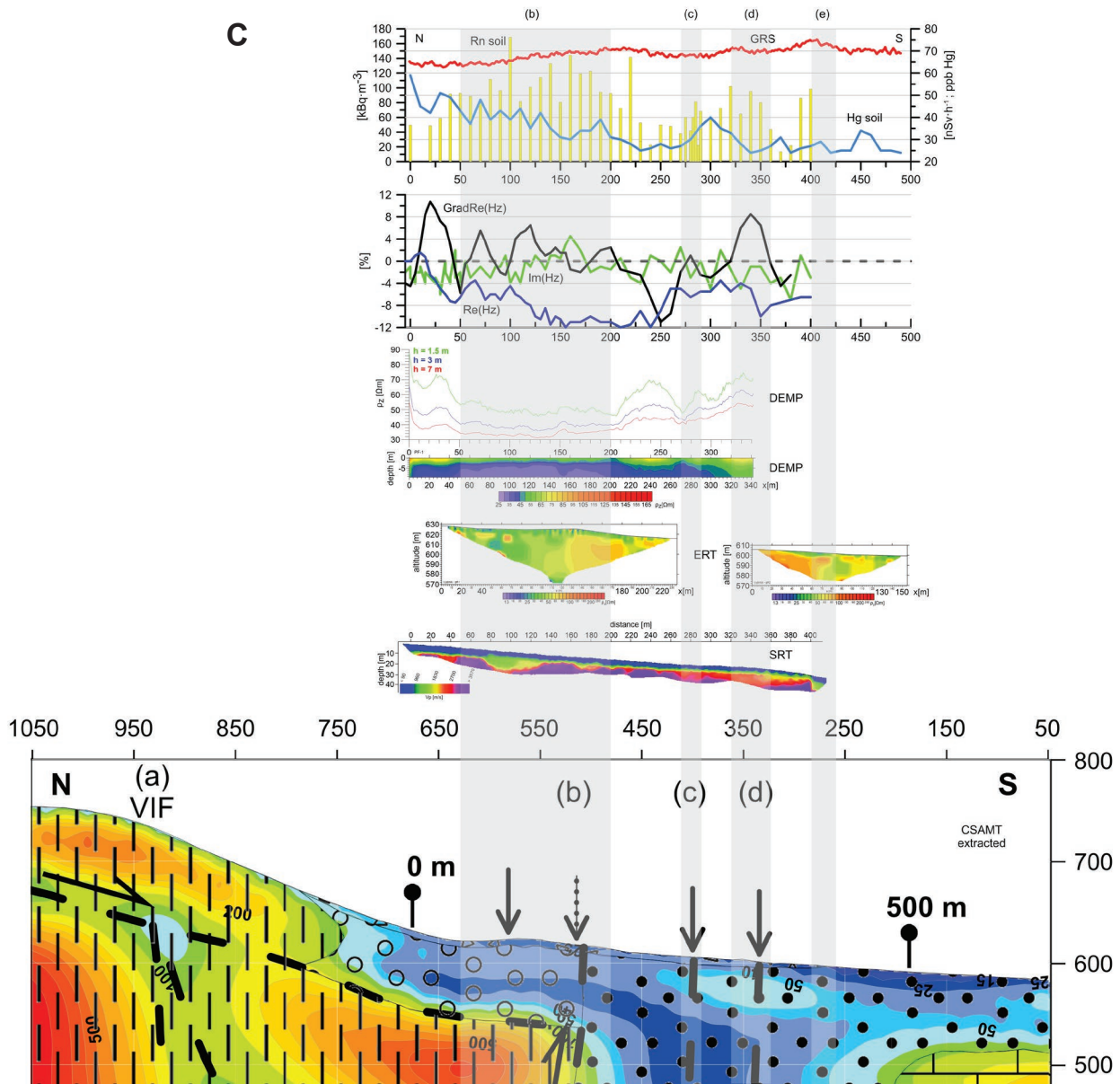
Fig. 5. (continued) Comparison of CSAMT related fault structures and shallow depth geophysical, emanometric and dowsing data. **A** — Kravany profile; **B** — Spišský Štiavnik profile; **C** — Vydrník profile; **D, E** — Spišské Bystré profiles; **F** — Hranovnica–Dubina profile. Geophysically detected single faults are distinguished by alphabet indications (a – VIFs.s., b, c, …) commented in the text. Grey transparent belts mark and connect multi-method indications of the same fault-discontinuity.

conditions in the northern part of the CSAMT profile the lines of shallow depth measurements do not cross the main northern VIF vertical dislocation (a), which occurrence emerges from the results of CSAMT measurements at surface stationing between 900–950 m (Fig. 4C).

Nevertheless, the shallow depth geophysical and emanometric surveys show they do cross the southern subvertical dislocation (b) discovered in the CSAMT cross-section at 500–510 m (Fig. 4C). This coincides with Mello et al. (2000) VIF interpretation in the geological map. Figure 5C highlights that this fault forms a discrete interface at 160–170 m in ERT

cross-section. This is the approximate centre of a 150 m wide fault damage zone (b) with low DEMP resistivity values at 50–200 m, a broad soil Rn anomaly between 40 and 200 m and positive VLF gradient Re(Hz) anomalies at 60–85, 100–155 and 180–205 m. The northern dowsing indication of this fault is supported by the highest soil radon activity concentration at 100 m with up to 168 kBq·m⁻³, a narrow vertical zone with the lowest ERT resistivity at 90 m and the SRT offset between 80 and 100 m (Fig. 5C).

While the highest positive VLF gradient Re(Hz) value anomaly at 10–40 m depicts the northern boundary of this

fault damage zone (b), the southern boundary is indicated by the high soil radon peak up to 140 kBq·m⁻³ and the channel of low ERT resistivity value at 220 m. This latter area is partly saturated by water which delivers higher conductivity and permeability for radon migration (Fig. 5C).

There are further likely southern parallel VIF offshoots: (c) at 270–290 m indicated by slightly higher soil radon values up to 81 kBq·m⁻³, lower DEMP resistivity and slightly positive VLF gradient value and (d) at 320–360 m, where there are high soil radon values up to 102 kBq·m⁻³ and a positive VLF gradient anomaly (Fig. 5C). Finally, higher soil radon values and lower ERT resistivity and SRT velocity values in their cross-sections provide fault indication at the southern end of the profile at 400 m (e). Both (c) and (d) offshoots have dowsing indication but not the (e) one (Fig. 4C).

Mercurometry and gamma-ray spectrometry can reflect bedrock lithology, but the methods reveal opposite values for the northern profile segment close to the sandy Ipoltica group at 0–200 m. This has higher soil Hg concentrations and lower gamma dose rate equivalent values than the southern segment in Paleogene clay sediments. Although the shallow-depth refraction seismic profile (SRT) does not unequivocally record VIF zone, there is Quaternary cover base at 80–100 and 400 m with decreased seismic wave velocity. This may indicate weakened zones in these positions, where the Quaternary cover depositions are distinguished from bedrock by their maximum 10 m thickness (Fig. 5C).

These weak anomalies are indicated by the VIF traces in the geological map and a fault discontinuity which marks the eastern extension of the VIF's western Kravany–Vydrník segment. A further discontinuity was detected in the Vydrník profile, and dowsing mapped its trace between Vydrník and Spišský Štiavnik. In addition, the CSAMT cross-section supports this fault in a small vertically-elongated low-resistivity anomaly at 200 m depth adjacent to the position initially detected by dowsing.

Spišské Bystré profiles (Fig. 5D, E)

The ERT, VES, SP, GRS and Rn soil geophysical methods were measured along two profiles in the surrounds of Spišské Bystré village (Figs. 3, 5D, 5E).

The eastern profile began in the steep slope of the Kozie chrbty Mts. and continued to the southern Hornád River alluvial plain (Fig. 5D). The ERT and VES resistivity sections distinguished the higher resistivity Permian sandstones in the 0–30 m northern sloped portion covered by stony scree and the lower resistivity Quaternary fluvial sediments (30–130 m) which cover the higher resistivity body of subsided Permian sandstones or buried stony scree at 30–100 m. The gamma dose rate equivalent further confirms this spatial lithological distribution by lower values of the more sandy soils up to 15 m in the northern part, and by higher values of the clayey remainder of the profile. The highest values in two parts (30–50 m and 90–110 m) confirm the highest clay content which could also indicate the presence of a loose fault zone.

ERT and VES then mark the main VIF position (a) at 20–45 m in the lowered resistivity portion. This is supported by the SP minimum at 25 m and most likely by the small soil radon maximum at 45 m. Two possible VIF offshoots are also indicated: (b) in electrical sections at 70–80 m, supported by the soil radon maximum at 60–80 m and the wide SP minimum at 50–75 m, and (c) by VES and ERT readings at 105–120 m and maximum soil Rn at 115 metres.

Figure 5E depicts the western profile running through a northern deep valley to the southern Hornád River alluvial plain. The northern part of the profile comprises Permian sandstones and shales with higher resistivity in ERT and VES sections and there is also a more compact deeper body with highest resistivity between 70 and 110 m (Fig. 5E). In contrast, the southern part of the profile is composed of Quaternary clayey-sandy sediments with low resistivity values. The main VIF position (a) is marked by their boundary at 110–120 m. The GRS depicts higher values in the Permian material distribution up to 160–170 m from valley creek flow. Three possible VIF offshoots are also indicated based on VES results, lower ERT resistivity and higher soil radon concentration values: (b) at 20–40 m, (c) at 70–90 m and (d) at 170–190 metres.

Hranovnica–Dubina profile (Fig. 5F)

The DEMP, VLF and magnetometry methods were used along the 250 m N–S oriented profile in the Hranovnica village surrounds (Fig. 3) initially indicated by physical dowsing. Figure 5F depicts these results, and while the northern part up to 130 m highlights the hill slope with more stony ground material, the southern portion is in the Hornád River alluvial plain (Fig 5F). The VIF determined by low 10 to 40 m DEMP resistivity supports our dowsing results, and the fault is further indicated by the VLF gradient Re(Hz) positive values commencing at 30 m and the magnetic field peaks at 10 and 40 metres. But the similar pattern of DEMP and magnetometry results at 90–100 m may be due to a road crossing the line at this site. Finally, the wide positive Re(Hz) gradient anomaly at 100–140 m establishes steep terrain increase at 105–125 m, and here the alluvial plain at the remainder of the profile has a monotonous environment with low resistivity.

Discussion

While it may not be widely accepted that soil radon values have a direct relationship to fault tectonic activity, we expect the studied fault zone to be permeable to volatiles, including radon. Therefore, we employed emanometry measurements of soil radon (Rn) and soil mercury (Hg). Most VIF detections herein have maximum soil radon values, although we expected even higher values, and interpretation of Hg results requires caution because we expected higher concentrations in the fault zones than measurements indicate. However, the weak Hg concentrations may indicate inability of volatiles to migrate in
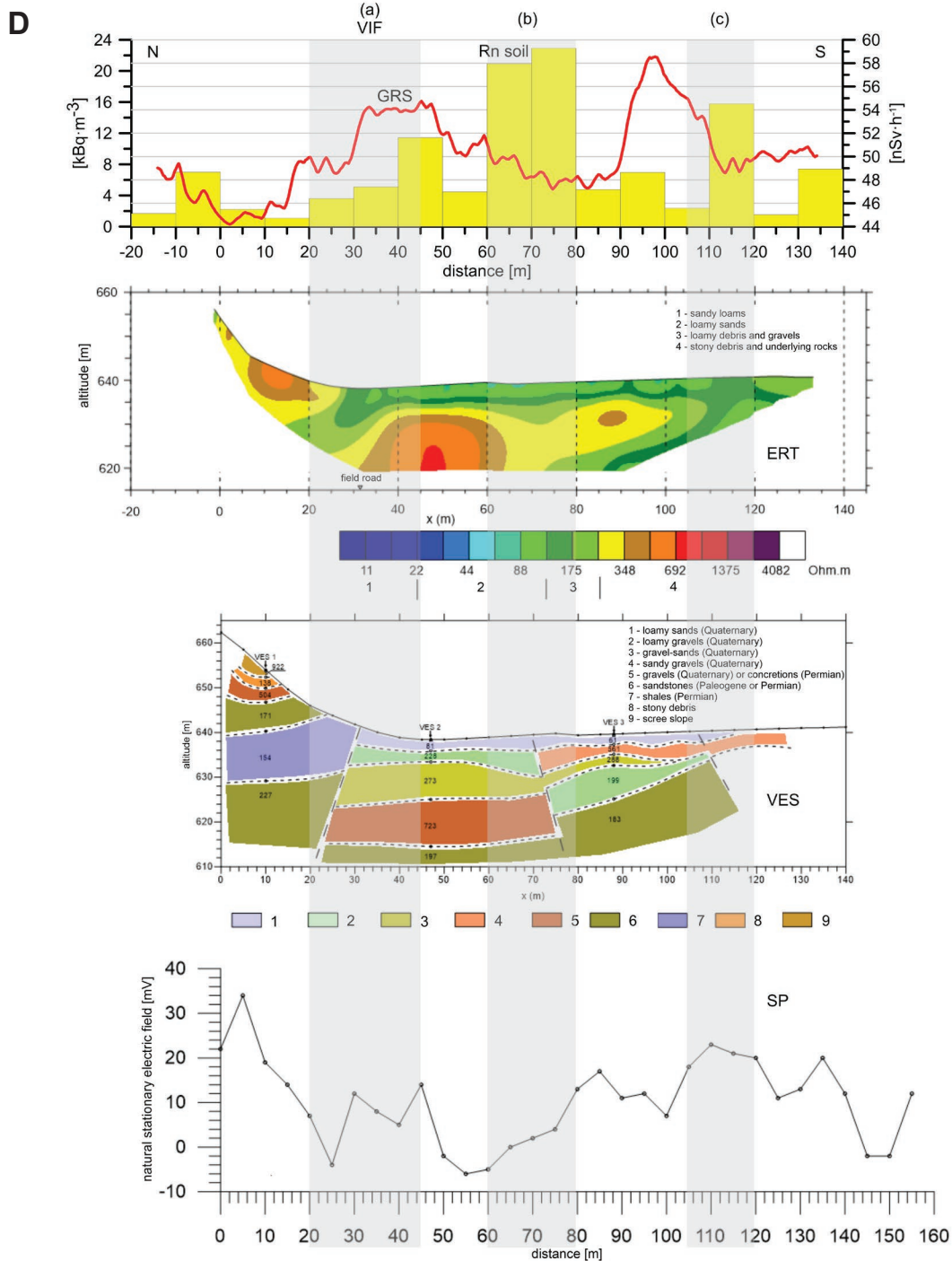
Fig. 5. (continued) Comparison of CSAMT related fault structures and shallow depth geophysical, emanometric and dowsing data. **A** — Kravany profile; **B** — Spišský Štiavnik profile; **C** — Vydrník profile; **D, E** — Spišské Bystré profiles; **F** — Hranovnica–Dubina profile. Geophysically detected single faults are distinguished by alphabet indications (a – VIFs.s., b, c, …) commented in the text. Grey transparent belts mark and connect multi-method indications of the same fault-discontinuity.

a closed fault zone because we observe this in reverse/compressional faults (Dadlez & Jaroszewski 1994). Moreover, the emanometry record is strongly influenced by basement lithological characteristics (clay content, ...), water saturation and the thickness of Quaternary cover deposition where

volatile concentrations are normally measured. Further investigation into these phenomena is necessary because of the complex interaction of factors influencing emanometry.

Faults have previously been considered drainage pathways for fluids and other volatiles. Therefore, it would be beneficial

for environmental, medical and economic purposes to detect and monitor fault concentrations of other volatiles such as CH_4 and CO_2 (Bigi et al. 2014). This could also be combined with surveys of fault zone water saturation and migration. The self-potential (SP) method assesses water filtration potential. Although this was applied only to the Spišské Bystré profile, it identified the minimum values of fault water-drainage to deeper parts (Fig. 5D). These SP measurements could also be assessed in the Vydrník profile because large underground water reserves and intensive drainage is assumed in the deeper parts of the faults (Fig. 4C).

Here, we employed the VLF which was abandoned due to the introduction of global positioning systems. Nevertheless, this method effectively detected the discontinuities in our research. The currently active IXZ and ICV VLF transmitters then enabled assessment of the VLF analogue device on the VIF trace. The positive values of calculated gradients of the Re(Hz) component of electromagnetic field were used as indicators of conductive fault zones.

The VIF parameters detected by our multi-method field surveys provided precise data with practical use. Additional scientific value here is found in the geodynamic explanation
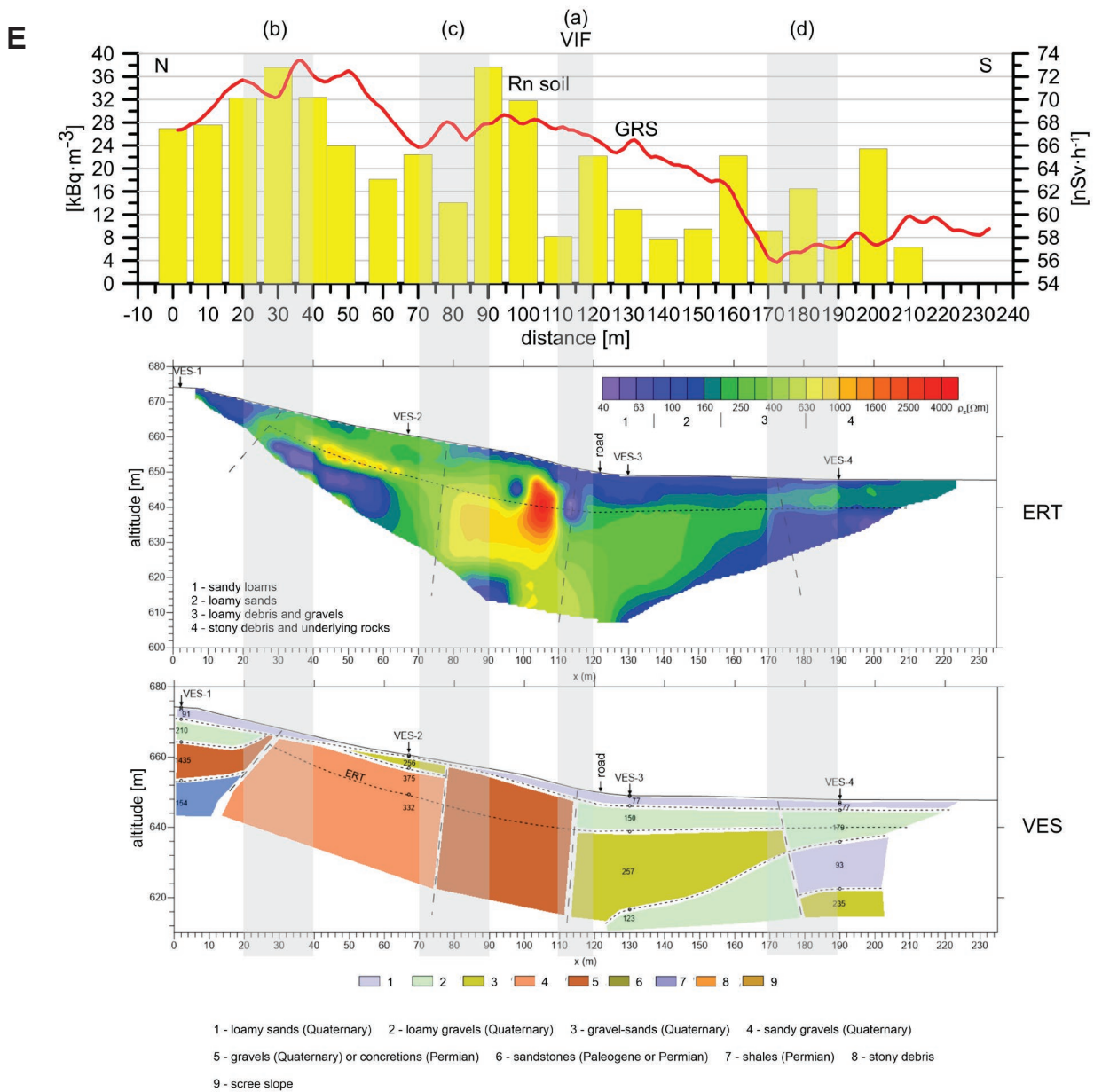

Fig. 5. (continued) Comparison of CSAMT related fault structures and shallow depth geophysical, emanometric and dowsing data. **A** — Kravany profile; **B** — Spišský Štiavnik profile; **C** — Vydrník profile; **D, E** — Spišské Bystré profiles; **F** — Hranovnica–Dubina profile. Geophysically detected single faults are distinguished by alphabet indications (a – VIFs.s., b, c, …) commented in the text. Grey transparent belts mark and connect multi-method indications of the same fault-discontinuity.
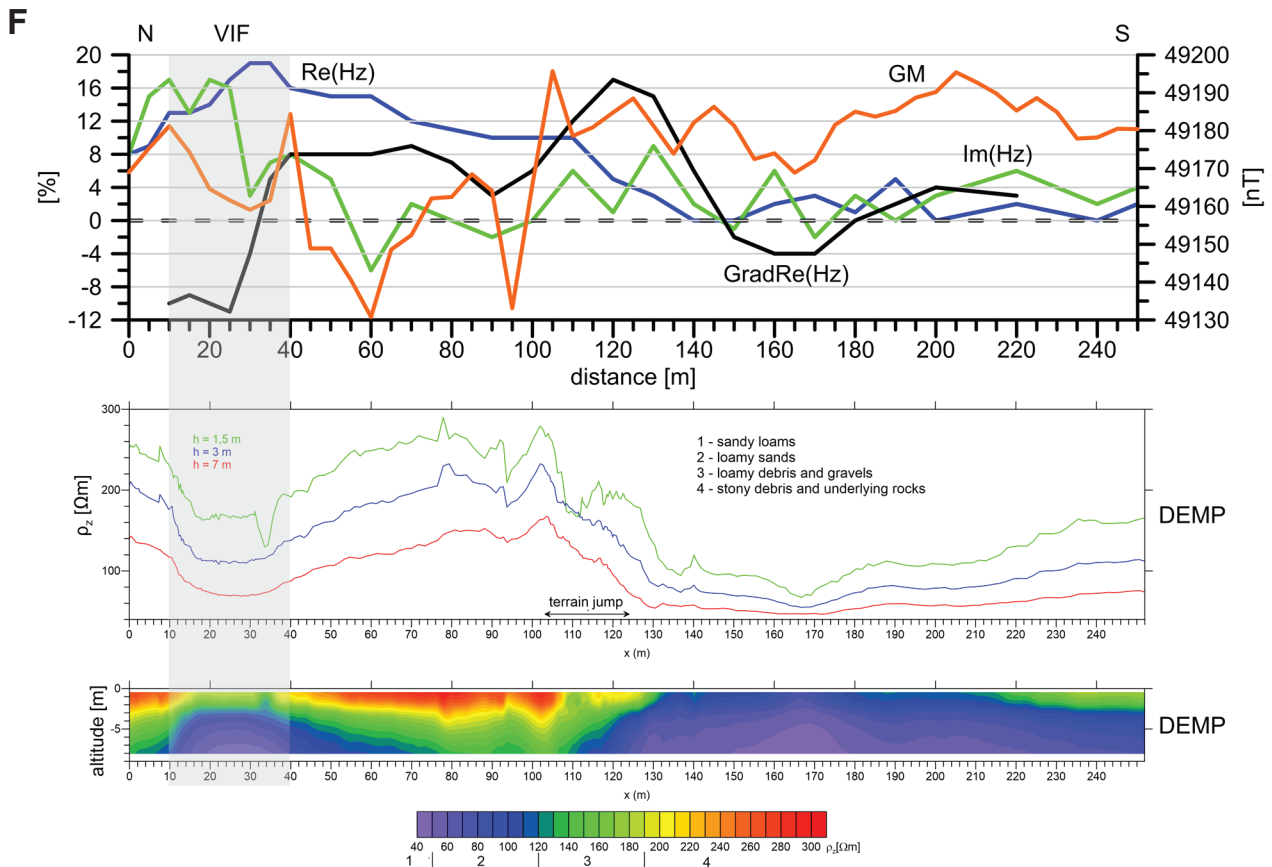
Fig. 5. (continued) Comparison of CSAMT related fault structures and shallow depth geophysical, emanometric and dowsing data. **A** — Kravany profile; **B** — Spišský Štiavnik profile; **C** — Vydrník profile; **D, E** — Spišské Bystré profiles; **F** — Hranovnica–Dubina profile. Geophysically detected single faults are distinguished by alphabet indications (a – VIFs.s., b, c, …) commented in the text. Grey transparent belts mark and connect multi-method indications of the same fault-discontinuity.

of fault kinematics and orientation, and the summary of their functions in geological evolution is contained in the VIF origin model (Fig. 6). Although fault inclination to the north identifies the dislocation's reverse character, this inclination is too steep from the point of geodynamics, because the ideal reverse fault inclination in classic stress-strain models under Mohr-Coulomb criteria is approximately 30° (Anderson 1951).

Therefore, we consider that the current VIF steep position is due to younger block tilting. In addition, analogous parameters and evolution are expected for the Sub-Tatras currently high-angle fault that originally operated as a reverse back-thrust fault (sensu Turcotte & Schubert 2014), and accommodated shortening from continent-continent collision (Fig. 6A). In contrast, Sperner et al (2002) consider that the cause is a transpressional reverse fault which restrains the sinistral strike-slip fault bridge. This Sub-Tatras fault later steepened and rotated with the Vysoké Tatry block due to block-tilting along the southern-dipping listric normal fault in the plane of the reactivated IWC thrust, or along shallower listric normal decollement (Fig. 6B). The kinematic fluctuation of IWC decollement from thrusting to normal faulting could have

occurred from slab retreat with steepening of the plate subducted under the Western Carpathians plates (Doglioni 1992).

While this model combines with the transpressional and extensional models of the Vysoké Tatry Mts. morpho-structural evolution in a continual process, the steep VIF position allows us to consider that it could also have operated as a strike-slip fault in a transpressional regime. Although this model could explain the Kozie Chrbty mountain ridge block uplift too, it does not elucidate the general northward dipping of geological units in the area, and this tectonic style can therefore only be interpreted as a result of tilting.

Concluding remarks

Our major goals in this study were to establish the following: (1) the most effective available field survey methods for map-scale fault detection in the terrain (2) determining their inclination with precise map-tracing and (3) establishing of the Vikartovce fault (Fig. 1) zone width and permeability for volatiles and water saturation. The research was based on a multi-method geophysical approach. The basic CSAMT

Table 1: Geographic coordinates of the survey profiles' marginal points.

Locality	Profile	Figure	GPS coordinates (from North to South)
Kravany	shallow geophysics	Figs. 3A, 5A	0 m: N49.005864 E20.209094 220 m: N49.00397 E20.20979
	CSAMT	Figs. 3A, 4A	300 m: N49.006439 E20.210738 −50 m: N49.003781 E20.210498
Spišský Štiavnik	shallow geophysics	Figs. 3B, 5B	0 m: N49.004246 E20.348517 200 m: N49.002464 E20.348298
	CSAMT	Figs. 3B, 4B	552 m: N49.005836 E20.351901 −90 m: N49.000861 E20.34769
Vydrník	shallow geophysics	Figs. 3C, 5C	0 m: N49.00568 E20.41422 500 m: N49.00129 E20.41496
	CSAMT	Figs. 3C, 4C	1200 m: N49.010496 E20.413614 −150 m: N48.998365 E20.415392
Spišské Bystré	shallow geophysics profile 1	Figs. 3D–E, 5D	0 m: N49.0079 E20.252023 150 m: N49.006547 E20.252106
	shallow geophysics profile 2	Figs. 3D–E, 5E	0 m: N49.008589 E20.250697 120 m: N49.007536 E20.250536
Hranovnica–Dubina	shallow geophysics	Figs. 3F, 5F	0 m: N49.005143 E20.323662 250 m: N49.003314 E20.324998
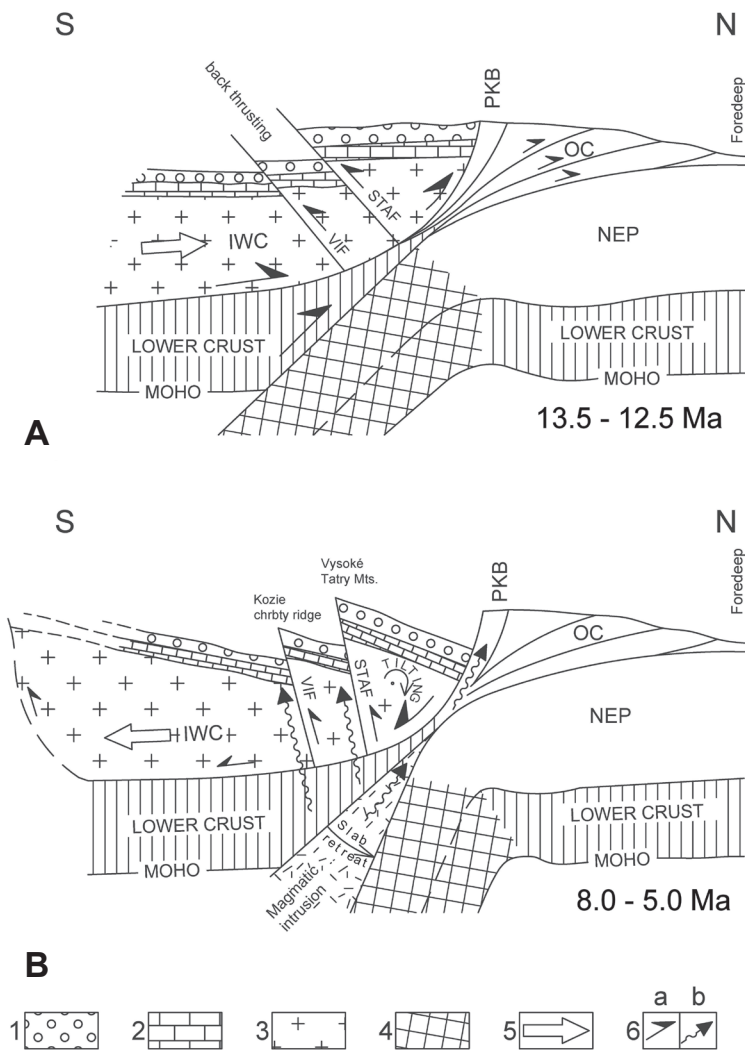
resistivity analysis provided information on deep geological structures, and we combined this with shallow-range geophysical methods to establish the near-surface horizon (Figs. 4 and 5). DEMP, ERT and VES geoelectrical resistivity then proved reliable in identifying sub-vertical and sub-horizontal boundaries, and these determined minimum resistivity values in the fault discontinuities. Additional procedures were beneficial, with seismic refraction tomography giving a clear picture of horizontal layering, but with less indication of subvertical elements except in the Kravany profile (Fig. 5A).

Ten field geophysical survey methods were applied with soil radon emanometry and mercurometry along five profiles crosscutting the studied fault trace (Fig. 3). In addition, we monitored indoor radon in selected Vydrník village houses constructed near the fault trace.

We then optimized field survey determination of map-scale fault characteristics, and combined the standard available shallow-depth field techniques and deep-range geophysical profiling. However, the shallow-depth methods alone do not provide the studied dislocations' precise location and geometric parameters (fault inclination), so we applied audio-magnetotelluric profiling to position the fault in cross-section and establish its inclination. Combining this with more superficial geophysical survey methods provided the most comprehensive data on map-scale faults.

We tested available field research methods in three extensive research seasons, and the experience gained promotes the following recommended approaches to detect map-scale faults:

• Study of the available geological data is the important first step. This provides the constraints on the initial field approximation of the fault's position, its three-dimensional parameters and geological interpretation of cross-section geophysics.

Fig. 6. Geodynamic evolution of the Sub-Tatras and Vikartovce faults – a conceptual scale-less model. **A —** back-thrusting from oblique continent-continent collision; **B —** block tilting due to orogene-perpendicular extension triggered by subducted plate steepening and retreat. 1. Inner Carpathian Paleogene Basin sediments, 2. Mesozoic nappe and cover units including Late Paleozoic complexes, 3. crystalline IWC basement, 4. oceanic crust, 5. plate movement vector, 6. a) fault kinematics, b) volatiles migration pathways. IWC – Inner Western Carpathians, NEP – North European Plate, PKB – Pieniny Klippen Belt, OC – Outer Carpathian accretionary flysch prism, VIF – Vikartovce Fault, STAF – Sub-Tatras Fault.

- The choice and precise location of the measurement lines are most important, and here, our dowsing profiling and mapping provided a rapid and cost-effective reconnaissance technique to detect fault trace in first approximation. However, we found it most beneficial when combined with VLF and DEMP measurements for initially defining precise fault position, and also the length of the profile cross-cutting the fault when the sedimentary cover was not too thick. Shallow depth measurements in the field then provided more suitable fault-line segments in thin Quaternary deposi-tions. In addition, the application of VES measurements in the early stages of fault research provided essential informa-tion on Quaternary deposition thickness.
- The next step requires choice of appropriate field survey methods and sequential scheduling of research procedures. We found that the best strategy is to concentrate all employed methods on a few promising profiles. Figure 5 shows that this gives the most comprehensive data and enables compa-rison of different method results.
- Following selection of the locality for fault parameter mea-surements, we recommend AMT/CSAMT measurements because MT results provide fundamental data to focus shal-low depth methods in the most promising parts of the profiles.
- Initial rapid surface geophysical methods including DEMP, VLF, magnetometry and GRS were applied in the desig-nated profiles.
- Those fast geophysical methods are then followed by more detailed geophysical survey by ERT, VES, SP, SRT, soil radon and mercury emanometry in important parts of the profile.

The choice of research procedures is strongly influenced by project budget. The most expensive are CSAMT measure-ments, but these are not only fundamental but also the most effective. Moreover, the MT cross-section results up to 1.2 km depth provided the most reliable data on the fault's position and incline. We highly recommend application of deep range VES measurements as well.

In conclusion, our multi-method research established novel and exact data on the Vikartovce fault's parameters (Figs. 4, 5), which allowed its genetic interpretation. This research con-firmed that the VIF is the fault interface between the Kozie chrbty Ridge and the Inner Carpathian Paleogene Basin filling in the Hornád depression. The VIF surface trace does not precisely follow the southern rim of the Kozie chrbty Horst, but it runs tens-of-metres southward at the Hornád depression pediment. Finally, we established that this tectonic steeply north-dipping contact has two tightly spaced parallel East-West sub-vertical dislocations – tilted reverse faults (Fig. 6) along which the horst of the Kozie chrbty Ridge is gradually uplifted some hundred metres against the Hornád depression Paleogene filling.

References

Anderson E.M. 1951: The dynamics of faulting. *Oliver and Boyd*, Edinburgh, 1–206.

Betz H.D. 1995: Unconventional Water Detection. Field Test of Dowsing Technique in dry Zones: Part 2. *Journal of Scientific Exploration* 9, 159–189.

Bezák V. (Ed.), Broska I., Ivanička J., Reichwalder P., Vozár J., Polák M., Havrila M., Mello J., Biely A., Plašienka D., Potfaj M., Konečný V., Lexa J., Kaličiak M., Žec B., Vass D., Elečko M., Janočko J., Pereszlényi M., Marko F., Maglay J. & Pristaš J. 2004: Tectonic map of Slovak republic 1:500,000. *ŠGÚDŠ*, Bratislava.

Bezák V. (Ed.), Elečko M., Fordinál K., Ivanička J., Kaličiak M., Konečný V., Kováčik M. (Košice), Maglay J., Mello J., Nagy A., Polák M., Potfaj M., Biely A., Bóna J., Broska I., Buček S., Filo I., Gazdačko Ľ., Grecula P., Gross P., Havrila M., Hók J., Hraško Ľ., Jacko S. ml., Jacko S. st., Janočko J., Kobulský J., Kohút M., Kováčik M. (Bratislava), Lexa J., Madarás J., Németh Z., Olšavský M., Plašienka D., Pristaš J., †Rakús M., Salaj J., Siman P., Šimon L., Teťák F., Vass D., Vozár J., Vozárová A. & Žec B. 2008: General geological map of Slovak republic 1:200,000. *ŠGÚDŠ*, Bratislava (in Slovak).

Bezák V., Majcin D., Klanica R., Vozár J. & Bilčík D. 2018: Nor-thernmost horst in the Neoalpine "horsts and grabens" structure of the Western Carpathians (Tatra and Ružbachy horst in the Northern Slovakia) in magnetotelluric data. In: *18th Internatio-nal Multidisciplinary Scientific GeoConference SGEM 2018: conference proceedings*. Vol. 18. *Applied and environmental geophysics*. STEF92 Technology, Sofia, 917–924.

Bielik M., Kloska K., Meurers B., Svankara J., Wybraniec S., Fancsik T., Grad M., Grand T., Guterch A., Katona M., Krolikowski C., Mikuška J., Pašteka R., Petecki Z., Polechonska O., Ruess D., Szalaiová V., Šefara J. & Vozár J. 2006: Gravity anomaly map of the CELEBRATION 2000 region. *Geologica Carpathica* 57, 145–156.

Biely M. 1989: The geological structure of the Western Carpathians. In: Maheľ, M., Dercourt, J. & Nairn, A.E.M. (Eds.): Evolution of the northern margin of Tethys. Vol. II. *Mémoires de la Société Géologique de France. Nouvelle Série* 154, Paris, 51-57.

Bigi S., Beaubien S.E., Ciotoli G., D'Ambrogi Ch., Doglioni C., Ferrante V., Lombardi S., Milli S., Orlando L., Ruggiero L., Tartarello M. & Sacco P. 2014: Mantle-derived CO_2 migration along active faults within an extensional basin margin (Fiumi-cino, Rome, Italy). *Tectonophysics* 637. https://doi.org/10.1016/j.tecto.2014.10.001

Dadlez R. & Jaroszewski W. 1994: Tectonics. *Wyd. Naukowe PWN*, Warszawa, 1–743 (in Polish).

Daynes J. 2012: The Dowsing and Geophysics Project at Moistown, Broadwoodkelly. Interim report 2012, ACE archaeology club, Great Britain. www.ACEarch.org.uk

Decker K., Meschede M. & Ring U. 1993: Fault slip analysis along the northern margin of the Eastern Alps (Molasse, Helvetic nappes, North and South Penninic flysch and the Norther Cal-careous Alps). *Tectonophysics* 223, 291–312. https://doi.org/10.1016/0040-1951(93)90142-7

Doglioni C. 1992: Main differences between thrust belts. *Terra Nova* 4, 152–164. https://doi.org/10.1111/j.1365-3121.1992.tb00466.x

Fiddick T. 2011: Dowsing: With an Account of Some Original Experiments. Sheffield, United Kingdom. *The Cornovia Press*, 1–3.

GCI & NFC, 2017–2019: Geodetic and Cartographic Institute Bratislava & National Forest Centre. 2017–2019. http://www.gku.sk/gku/, https://web.nlcsk.org/

Geofyzika, n.p. 1978: VLF instrument EDA 78 – ERA 77. Working instructions. Brno, Czechoslovakia, 1–43 (in Czech).

Gross P. 1973: About the Choč – Sub-Tatras fault. *Geologické Práce, Správy* 61, 315-319 (in Slovak).

Gross P., Buček S., Ďurkovič T., Filo I., Karoli S., Maglay J., Nagy A., Halouzka R., Spišák Z., Žec B., Vozár J., Borza V., Lukáčik E., Mello J., Polák M. & Janočko J. 1999: Geological map of Popradská kotlina Basin, Hornádska kotlina Basin, Levočské vrchy Mts., Spišsko-šarišské medzihorie Depression, Bachureň Mts. and Šarišská vrchovina highland (scale 1:50,000). *Ministry of Environment of Slovak Republic, Geological Survey of Slovak republic*, Bratislava.

Gross P., Kohler E. & Samuel O. 1984: A new litho-stratigraphic division of the intra-Carpathian Paleogene. *Geologické Práce, Správy* 81, 103–119 (in Slovak).

Jakál J. 1992: Influence of neotectonics on development of river network changes in the Low Tatra Mts. and the Podtatranská kotlina basin (Locality: 5). In: Stankoviansky M. & Lacika J.: Excursion guide-book. *Intern. Symposium Time, Frequency and Dating Geomorphology*, Tatranská Lomnica, June 16–21, 1992, 42–45.

Janák M., Plašienka D. & Petrík I. 2001: Excursion to the Tatra Mountains, Central Western Carpathians: Tectonometamorphic Records of Variscan and Alpine Orogeny. *Geolines* 13, 141–148.

Jurewicz E. 2005: Geodynamic evolution of the Tatra Mts. and the Pieniny Klippen Belt (Western Carpathians). *Acta Geologica Polonica* 55, 295–338.

Keith J.F. jun., Nemčok M., Fleischmann K.H., Nemčok J., Gross P., Rudinec R. & Kanes W.H. 1991: Sedimentary basins of Slovakia, part III. Hydrocarbon potential of the Central Carpathian Paleogene Basin. Vol. I*., Res. Report*, *MS, ŠGÚDŠ* Bratislava, *Maxus Energy Corporation*, 1–133.

Kowalski W.C. 1996: Dowsing and radiesthesia; to test or not to test, that is the question. *Przeglad Geologiczny* 44, 39–42.

Landa V.E. & Kovalevsky A.L. 1997: Integration of dowsing with biogeochemical and electrical prospecting techniques at gold ore deposits. *Bulletin of Dowsing* 8, 9–12.

Lillie R.J. 1999: Whole Earth Geophysics. *Prentice Hall*, New Jersey, 1–361.

Lohmann H.H. 1998: Dowsing versus geophysics. *Bulletin for Applied Geology* 3, 199–203.

Lukniš M. 1973: Relief of the Vysoké Tatry Mts. and their foreland. *Vydavateľstvo SAV* Bratislava, 1–345 (in Slovak).

Maglay J., Halouzka R., Baňacký V., Pristaš J. & Janočko J., 1999: Neotectonic map of Slovakia. *GSSR*, Bratislava (in Slovak).

Maheľ M. 1986: Geological architecture of the Czecho-slovakian Carpathians 1 – Paleo-Alpine units. *Veda*, Bratislava, 1–508 (in Slovak).

Mareš S., Karous M., Landa I., Mazač O., Müller K. & Müllerová J. 1983: Geophysical methods in hydrogeology and engineering geology. *SNTL/ALFA*, Prague, 1–199 (in Czech).

Mareš S., Gruntorád J., Hrách S., Karous M., Marek F., Matolín M. & Skopec J. 1984: Introduction to Applied Geophysics. *D. Reidel Publishing Company*, Dordrecht, 1–581.

Marko F. l996: Dynamic analysis of fault deformations of the Central Carpathian Paleogene basin based on structural observations from the north-western and southern periphery of the Levočské vrchy Mts. In: Soták J. (Ed.) 1996: Zhodnotenie geologickej stavby Levočských vrchov. Čiast. záv. správa úlohy „Flyš východného Slovenska – geofyzika, štúdia". *Manuscript, GÚ SAV B. Bystrica*, 1–1193 (in Slovak).

Marko F. 2002: Faults and their role during the Tertiary evolution of the Western Carpathians (ALCAPA region). *Habilitation thesis*, *PriF UK Bratislava*, 1–88 (in Slovak).

Marko F., Andriessen P.A.M., Tomek Č., Bezák V., Fojtíková L., Bošanský M., Piovarči M. & Reichwalder P. 2017: Carpathian Shear Corridor – A strike-slip boundary of an extruded crustal segment. *Tectonophysics* 703–704, 119–134. https://doi.org/10.1016/j.tecto.2017.02.010

Marko F., Dyda M., Gajdoš V., Rozimant K. & Mojzeš A. 2015: Buried faults mapping – a new field approach applied in the Western Carpathians. *Geological Quarterly* 59, 35-46. https://doi.org/10.7306/gq.1199

Marko F., Preusser F., Vojtko R., Madarás J. & Kováčová M. 2010: A contribution to dating Quaternary faults (Vikartovce fault, Western Carpathians). In: Kohút M. (Ed.): DATING 2010. *Conf. Proceeds., Konferencie, Sympóziá, Semináre, ŠGÚDŠ*, Bratislava, 23-24.

Marschalko R., Gross P. & Kalaš L. 1966: Paleogene and Quaternary of the Hornádska kotlina depression. *Geologické práce, Zprávy* 39, 95–104 (in Slovak).

Mello J. (Ed.), Filo I., Havrila M., Ivanička J., Madarás J., Németh Z., Polák M., Pristaš J., Vozár J., Koša E. & Jacko S. jun. 2000: Geological map of the Slovenský raj, Galmus and Hornádska kotlina depression. *ŠGÚDŠ*, Bratislava (in Slovak).

Mičian Ľ. 1962: A few notes to break of Hornád river in the Stratenská Hornatita Mts. and to morphology of surroundings. *Geografický Časopis* 14, 57–65 (in Slovak).

Milsom J. & Eriksen A. 2011: Field Geophysics. *Wiley*, 1–287. https://doi.org/10.1002/9780470972311

Mojzeš A., Marko F., Porubčanová B. & Bartošová A. 2017: Radon measurements in an area of tectonic zone: A case study in Central Slovakia. *Journal of Environmental Radioactivity* 166, 278–288. https://doi.org/10.1016/j.jenvrad.2016.08.012

Moldovan I.A., Apostol A., Moldovan A., Ionescu C. & Placinta A.O. 2013: The biolocation method used for stress forecasting in Vrancea (Romania) seismic zone. *Romanian Reports in Physics* 65, 261–270.

Nemčok J., Bezák V., Janák M., Kahan Š., Ryka W., Kohút M., Lehotský I., Wieczorek J., Zelman J., Mello J., Halouzka R., Raczkowski W. & Reichwalder P. 1993: Explanations to geological map of the Tatras Mts. 1:50,000. *GÚDŠ*, Bratislava, 1–135 (in Slovak).

Nemčok J., Bezák V., Biely A., Gorek A., Gross P., Halouzka R., Janák M., Kahan Š., Kotansky Z., Lefeld J., Mello J., Reichwalder P., Raczkowski W., Roniewicz P., Ryka W., Wieczorek J. & Zelman J. 1994: Geological map of the Tatras Mts. 1: 50,000. *ŠGÚDŠ*, Bratislava (in Slovak).

Pašteka R., Zahorec P., Kušnirák D., Bošanský M., Papčo J., Szalaiová V., Krajňák M., Marušiak I., Mikuška J. & Bielik M. 2017: High resolution Slovak Bouguer gravity anomaly map and its enhanced derivative transformations: new possibilities for interpretation of anomalous gravity fields. *Contributions to Geophysics and Geodesy* 47, 81–94. https://doi.org/10.1515/congeo-2017-0006

Peresson H. & Decker K. 1997: Far-field effects of Late Miocene subduction in the Eastern Carpatians: E-W compression and inversion of structures in the Alpine– Carpathian Pannonian region. *Tectonics* 16, 38–56. https://doi.org/10.1029/96TC02730

Pico Envirotec Inc. 2014: PGIS – 2. User´s Quick Reference Manual. Portable Ground Information System. *Concord*, Ontario, Canada, 1–23.

Pivko D. & Vojtko R. 2021: A review of travertines and tufas in Slovakia: Geomorphology, environments, tectonic pattern, and age distribution. *Acta Geologica Slovaca* 13, 49–78.

Reynolds J.M. 1997: An Introduction to Applied and Environmental Geophysics. First Edition, *John Wiley and Sons Ltd*, Chichester, 1–796.

Roth Z. 1938: Geological conditions in the surroundings of the Lučivná under the Vysoké Tatry Mts. *Rozpravy II. Tř. České akademie* 48/13, 1–28 (in Czech).

Sandmeier K.J. 2017: Reflexw – GPR and seismic processing software. Sandmeier geophysical research 2017. Available online: http://www.sandmeier-geo.de/reflexw.htm [Accessed 2018-01-04]

Smetanová I., Mojzeš A., Marko F., Fekete K. & Csicsay K. 2019: Indoor radon monitoring in selected fault zones, Slovakia – preliminary results from the summer monitoring period. *Contributions to Geophysics and Geodesy* 49, 391–402. https://doi.org/10.2478/congeo-2019-0020

Smetanová I., Mojzeš A., Csicsay K. & Marko F. 2022: Indoor radon monitoring in selected buildings in Vydrník (Vikartovce fault, Slovakia). *Radiation Protection Dosimetry* 198, 785–790. https://doi.org/10.1093/rpd/ncac133

Sperner B. 1996: Computer programs for the kinematic analysis of brittle deformation structures and the Tertiary tectonic evolution of the Western Carpathians (Slovakia). *Tübinger Geowiss. Arb.*, Reihe A 27, 1–120.

Sperner B., Ratschbacher L. & Nemčok M. 2002: Interplay between subduction retreat and lateral extrusion: Tectonics of the Western Carpathians. *Tectonics* 21, 1–24. https://doi.org/10.1029/2001TC901028

Sůkalová Ľ. 2010: Evolution of the Cenozoic paleostress field in the western part of the Hornádska kotlina depression and Kozie chrbty ridge. *Mgr. thesis, Dept. of geology and paleontology PRIF UK*, Bratislava, 1–90 (in Slovak).

Tomek Č. 1993: Deep crustal structure beneath the central and inner West Carpathians, *Tectonophysics* 226, 417–431. https://doi.org/10.1016/0040-1951(93)90130-C

Turcotte D. & Schubert G. 2014: Geodynamics. Third edition, *Cambridge University press*, 1–623. https://doi.org/10.1017/CBO9780511843877

Twiss J.R. & Moores M.E. 1992: Structural geology. *W. H. Freeman Company*, New York, 1–532.

Vass D. 1998: Neogene geodynamic development of the Carpathian arc and associated basins. In: Rakús M. (Ed.): Geodynamic development of the Western Carpathians. GSSR, *Dionýz Štúr Publishers*, Bratislava, 155–158.

Vojtko R., Marko F., Preusser F., Madarás J. & Kováčová M. 2011: Evidence for Late Quaternary uplift along the Vikartovce Fault (Western Carpathians, Slovakia). *Geologica Carpathica* 62, 563–574. https://doi.org/10.2478/v10096-011-0040-9

Vozárová A. & Vozár J. 1988: Late Paleozoic in West Carpathians. *Geological Institute of Dionýz Štúr*, Bratislava, 1–314.

Udič M. 2010: Structural-tectonic evolution of the sub-Tatras – Ružbachy fault system. *PhD. thesis*, *BERG Faculty, TU Košice*, 1–109 (in Slovak).